Results in Materials 21 (2024) 100546

Contents lists available at ScienceDirect

Results in Materials

journal homepage: www.sciencedirect.com/journal/results-in-materials

Corrosion behaviour of cobalt-based coatings with ruthenium additions in synthetic mine water

Silas I. Hango [a,b,*], Lesley A. Cornish [a], Josias W. van der Merwe [a], Lesley H. Chown [a], Frank P.L. Kavishe [b]

[a] School of Chemical and Metallurgical Engineering, DSI-NRF Centre of Excellence in Strong Materials and African Materials Science and Engineering Network (AMSEN): Hosted by the University of the Witwatersrand, Private Bag 3, WITS, 2050, Johannesburg, South Africa
[b] Department of Mechanical and Metallurgical Engineering, University of Namibia, P.O. Box 3624, Ongwediva, Namibia

ARTICLE INFO

Keywords:
Cobalt-based alloys
Coatings
Ru additions
Corrosion
Potentiodynamic polarisation
Passivation

ABSTRACT

The corrosion behaviour of two cobalt-based coatings (ULTIMET™ and STELLITE™ 6) with zero, 0.3 and 0.6 wt % ruthenium were studied and compared with two cobalt-based bulk alloys (ULTIMET™ and STELLITE™ 6B) in synthetic mine water (pH values of 6, 3 and 1) using potentiodynamic polarisation. The coatings demonstrated wider ranges of passivation behaviour (from −250 mV to 750 mV) than the bulk alloys. The corrosion potential became more positive and the active-passive transition reduced with increased Ru. The best coating was STELLITE™ 6 with 0.6 wt% Ru, which exhibited the lowest corrosion rates: 3.6 μm/y at pH 6 and 6.4 μm/y at pH 3.

1. Introduction

Cobalt-based alloys and coatings, such as Co–Cr–Ni–Mo and Co–Cr–W–Fe are used to protect mild steel in many industrial applications, including slurry pump components such as casings, sleeves and valves, as well as physiological or orthopaedic implants such as artificial knees and hips, owing to the their excellent mechanical properties and resistance to corrosion [1,2]. They are also used in applications such as cutting tools, hard-facing castings, and in various industries, including power generation, oil and gas, steel manufacturing, chemical processing and marine environments [2]. The predominant alloys comprise cobalt, with chromium to reinforce the cobalt matrix, facilitate the formation of chromium carbide (Cr_3C_2) and establish a defensive passive layer of chromium oxide (Cr_2O_3). Additionally, tungsten (W) is occasionally employed to enhance hardness [3,4], e.g., ULTIMET™ (Co–Cr–Ni–Mo–Fe–W–Mn–Si–N–C) and STELLITE™ 6 (Co–Cr–W–Fe–Ni–Mo–Mn–Si–C), which are commercially available as for corrosion and wear resistant coatings on steels [4–7]. These coatings spontaneously passivate in various environments, which is observed at open circuit potentials or at certain anodic polarisations [8]. The passivation behaviour of these coatings may be cathodically modified by adding a very small amount of ruthenium to increase corrosion resistance and wear resistance [9,10]. Ruthenium is used more than other the platinum group metals (PGMs), since it is the least expensive metal of that group, is more available in South Africa [10,11] and has a better solubility in the Co, Cr matrix than other PGM or precious metals [12]. With cathodic modification and with increased ruthenium content, corrosion potential increases to more noble values with a wide range of spontaneous passivation [13,14].

While iron-, nickel- and cobalt-based alloys have been extensively studied for their corrosion behaviour, other studies were on the effect of ruthenium (Ru) additions to hard metals to improve corrosion and wear resistance [11,12,14–16]. There has been limited research on the effect of small additions of Ru to cobalt-based alloys. Thus, the purpose of this study was to investigate and understand the corrosion behaviour of two different cobalt-based commercial ULTIMET™ and STELLITE™ 6B bulk alloys and ULTIMET™ and STELLITE™ 6 coatings cathodically modified with small additions of Ru (0, 0.3 and 0.6 wt% Ru) on mild steel, This was done using potentiodynamic polarisation in synthetic mine water to select the best performing coating and alloys to protect mild steel from corrosion in the test solutions. The small Ru additions were intended to enhance the corrosion resistance and hardness of the cobalt-based coatings.

* Corresponding author. Department of Mechanical and Metallurgical Engineering, University of Namibia, P.O. Box 3624, Ongwediva, Namibia.
E-mail address: shango@unam.na (S.I. Hango).

https://doi.org/10.1016/j.rinma.2024.100546
Received 30 November 2023; Received in revised form 26 January 2024; Accepted 7 February 2024
Available online 20 February 2024

Table 1
Composition of synthetic mine water solution used in the tests [17].

Salt	Concentration ($mg{\cdot}L^{-1}$)
$MgSO_4$	198
Na_2SO_4	1215
$CaCl_2$	1038
NaCl	1379

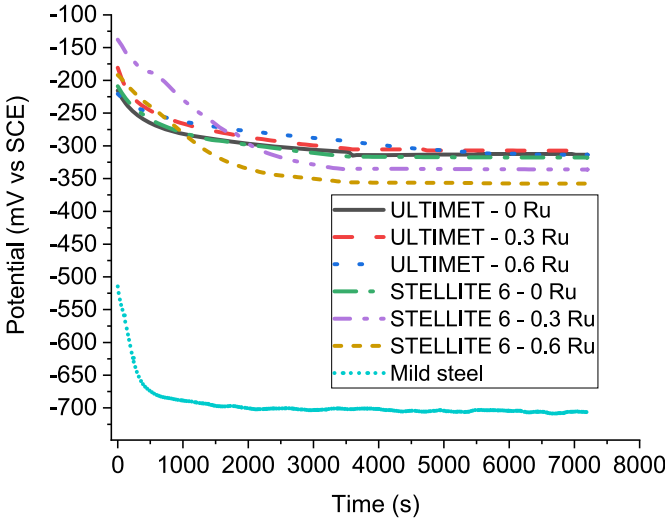

Fig. 1. Open circuit potentials of the ULTIMET™ and STELLITE™ 6 coatings with 0 Ru, 0.3 wt% Ru and 0.6 wt% Ru coatings and mild steel in synthetic mine water at pH 1.

2. Experimental details

2.1. Materials

The bulk alloys studied were ULTIMET™ and STELLITE™ 6B, supplied as bars by Multi Alloys, South Africa. Their corrosion behaviour was compared with that of the coatings, produced by mixing ULTIMET™ (Weartech Pty (Ltd), South Africa) or STELLITE™ 6 (Weartech Pty (Ltd) and Fe Powder Supplies (Pty) Ltd, South Africa) powder with either 0.3 or 0.6 wt% Ru, and coatings without Ru. The powders were thermally sprayed on to ASTM A516 mild steel substrates using a high velocity oxygen fuel (HVOF) technique with a FANUC™ System R-J3iB connected to a FANUC robot R-200 iA 16SF. The characterisation (microstructures and X-ray diffraction) of the cobalt-based alloys and coatings with ruthenium additions and hardness testing were described elsewhere [2].

2.2. Electrochemical tests

Synthetic mine water of the composition given in Table 1 was prepared by dissolving the salts in de-ionised water to produce a test solution of pH 6, and acidified with 32% HCl to pH values of 3 and 1. The corrosion behaviour of the samples was investigated in these solutions at 22.3 ± 1.0 °C. The measurements were carried out in a 500 ml three-electrode cell with the sample as the working electrode, a saturated calomel electrode (SCE) as the reference electrode which was placed in a Luggin capillary (to minimise errors due to ohmic drop) with a KCl solution salt-bridge and a graphite counter electrode. Samples were connected to a copper wire by aluminium conducting tape before being cold-mounted in epoxy resin for 12 h at room temperature, then wet ground from 80 to 1200 silicon carbide papers, washed with running de-ionised water, degreased with ethanol and dried in air. The areas of the samples exposed to the corrosive environment were measured, and each was aimed to be 1 cm^2. Prior to scanning, all samples were immersed in the test solutions for 2 h to stabilise the open circuit potential (OCP). The potentiodynamic polarisation measurements were performed using an

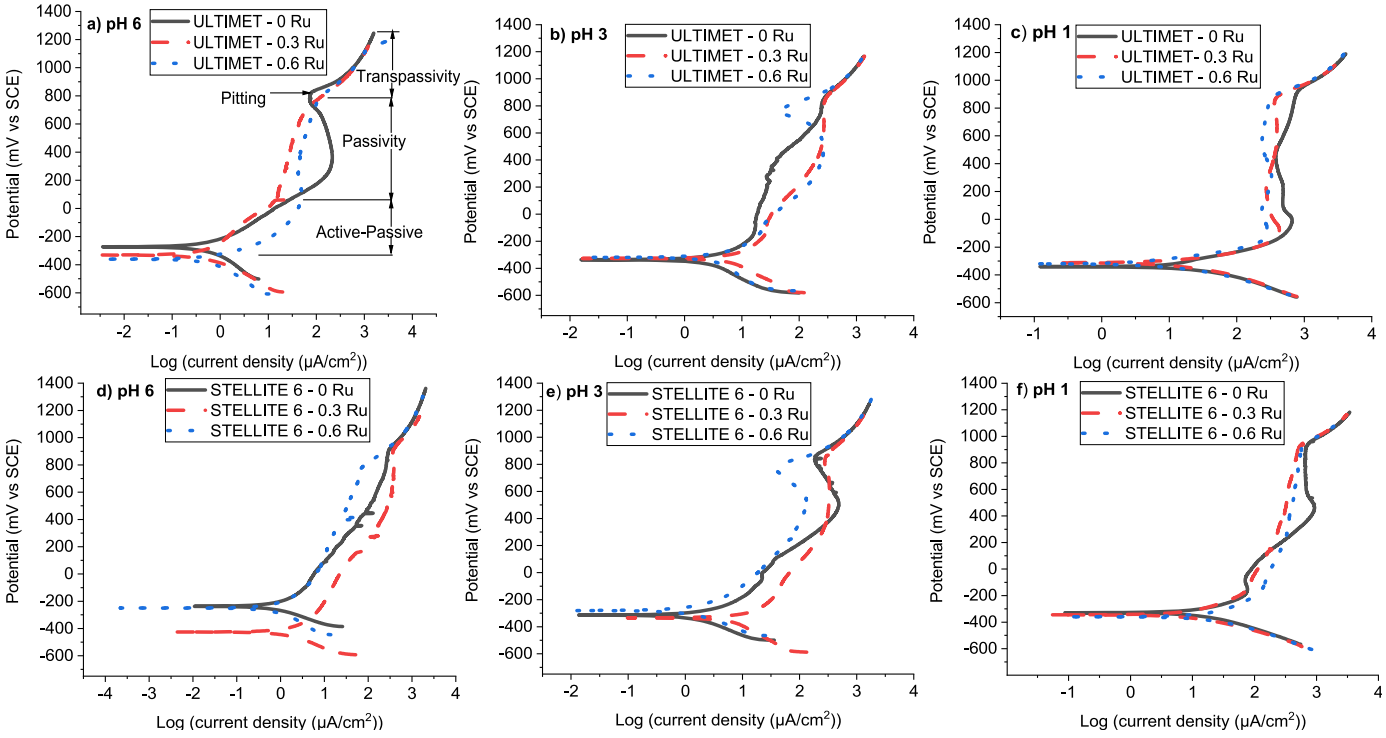

Fig. 2. Potentiodynamic polarisation curves of: (a–c) ULTIMET™ and d)-f) STELLITE™ 6 coatings, showing active, passive and pitting behaviour in synthetic (pH 6) and acidified synthetic (pH 3 and 1) mine water.

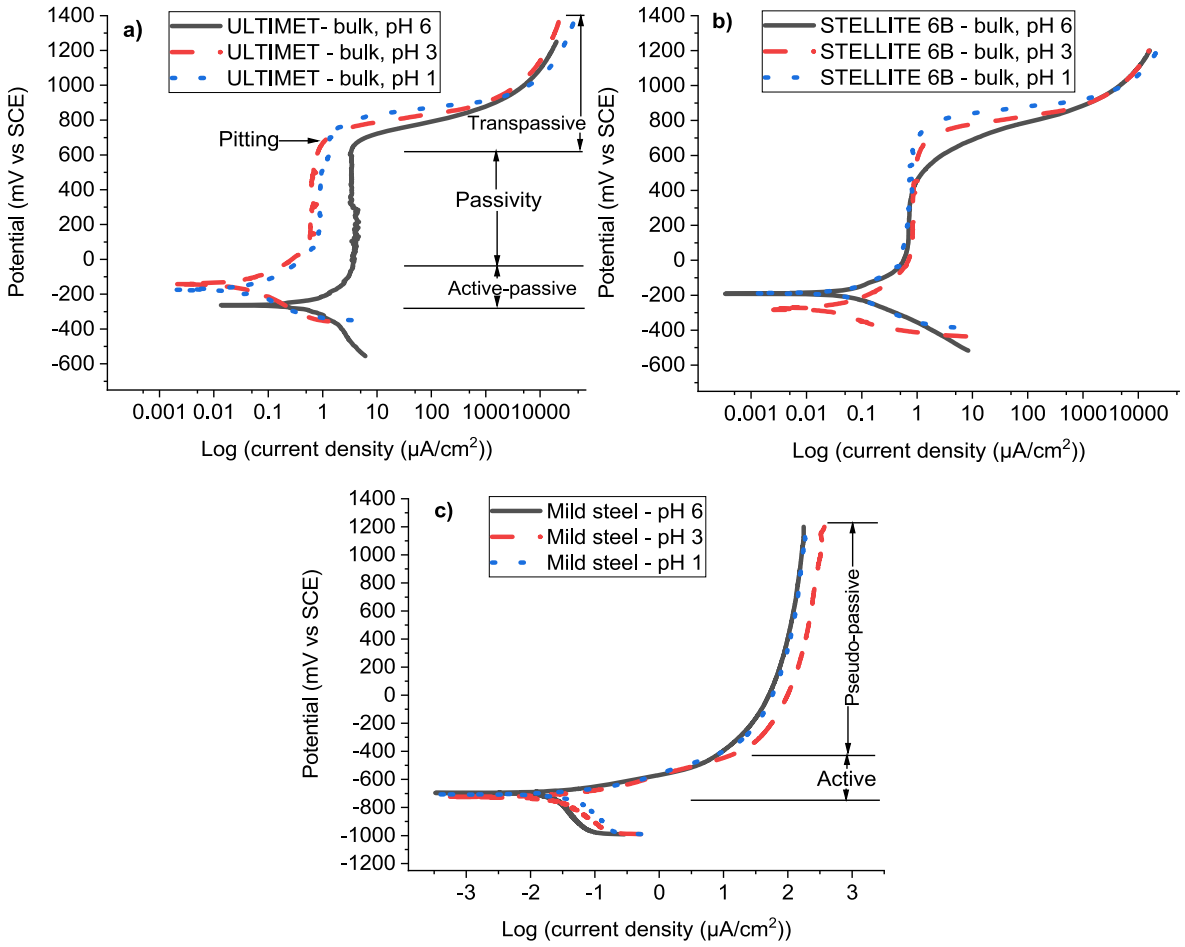

Fig. 3. Potentiodynamic polarisation curves of: (a) ULTIMET™, (b) STELLITE™ 6B and (c) mild steel in synthetic and acidified synthetic mine water, showing active and pseudo-passive behaviour.

Auto Tafel Potentiostat with Auto Tafel V1.79 and Auto LPR V2.7 h software at a scan rate of 0.2 mV·s^{-1} between −750 and 1200 mV versus the reference electrode potential after OCP scan. All tests were carried out in duplicate for reproducibility, and there were no significant differences between duplicates.

Linear polarisation resistance (R_p), measured ± 25 mV relative to the corrosion potential (E_{corr}), was used to calculate the corrosion rates of the samples. The corrosion current densities were calculated from values obtained from the polarisation resistance measurements. After polarisation, each sample was examined using optical and scanning electron microscopy to study the surface morphologies and films on the surface.

3. Results

The results of the particle sizes and surface morphologies of the powders, energy dispersive X-ray and X-ray diffraction results of the powders, alloys and coatings, surface morphologies of the coatings and hardness of the cobalt-based alloys and coatings with ruthenium additions were given elsewhere [2].

3.1. Open circuit potential measurements of the bulk alloys and coatings

The open circuit potentials (OCPs) of the ULTIMET™ and STELLITE™ 6 coatings and ASTM A516 mild steel substrate at pH 1 became more negative during the first 2000 s, and then nearly stabilised after ~4000 s (Fig. 1). This showed that stable passive films formed on their surfaces or possibly the saturation of ions in the electrolyte reduced the potentials. When Ru was added, OCP increased to less negative values for the ULTIMET™ coatings, while for STELLITE™ 6 coatings, OCP decreased to more negative values. This indicated that ULTIMET™ coatings formed the more stable and better passivating oxide films than STELLITE™ 6 coatings in the test solutions [8]. The OCP for mild steel decreased to more negative potentials than those of STELLITE™ 6 coatings, and thus the mild steel was much more susceptible to corrosion.

3.2. Potentiodynamic polarisation measurements of the bulk alloys and coatings

Fig. 2 presents potentiodynamic polarisation curves of the ULTIMET™ (Fig. 2 a-c) and STELLITE™ 6 coatings (Fig. 2 d-f) with different amounts of Ru in synthetic mine water (pH 6, 3 and 1). At all pH values, coatings displayed spontaneous active-passive transitions along with the stable current density. After E_{corr}, active-passive behaviour was observed for both coatings, and the significant increases both in potential and current density (i.e., active behaviour) suggested that protective films of Cr_2O_3 (i.e., passivity [3,18,19]) formed as current density remained unchanged for a range of potentials (passive behaviour). All curves showed an extended range of passivity from ~ −350 mV to over 1200 mV (Fig. 2), indicating protective films were formed. The passive behaviour changed around 750 mV–1200 mV due to pitting when the protective thin film was locally broken, which increased the current densities at these corrosion potentials [3,20]. Since the passive to the transpassive regions of the polarisation curves (Fig. 2) were similar for the different coatings (apart from the 0 wt% Ru coatings), the corrosion resistances of the coatings were very similar.

Table 2
Potentiodynamic polarisation results of ULTIMET™ and STELLITE™ 6 coatings, ULTIMET™ and STELLITE™ 6B bulk alloys, and mild steel substrate in synthetic and acidified synthetic mine water.

Coating (wt% Ru) and bulk alloy	pH	E_{corr} (mV)	i_{corr} (μA/cm^{-2})	R_p (Ω·cm^2)	Corrosion rate (μm/y)
ULTIMET™ - bulk	6	−263 ± 2	0.50 ± 0.00	43,522 ± 20	5.3 ± 1.3
	3	−143 ± 1	0.37 ± 0.00	56,510 ± 13	3.6 ± 0.3
	1	−177 ± 2	0.42 ± 0.00	47,600 ± 21	4.1 ± 0.0
ULTIMET™ - 0 Ru	6	−273 ± 2	0.26 ± 0.00	80,967 ± 17	3.1 ± 0.7
	3	−337 ± 2	1.46 ± 0.01	14,848 ± 66	15.3 ± 2.1
	1	−339 ± 0	13.20 ± 0.80	1643 ± 13	137.1 ± 5.0
ULTIMET™ - 0.3 Ru	6	−331 ± 1	0.24 ± 0.00	90,533 ± 25	3.0 ± 0.3
	3	−327 ± 1	3.91 ± 0.20	5542 ± 71	41.3 ± 4.0
	1	−313 ± 1	8.58 ± 0.10	2548 ± 27	89.2 ± 4.1
ULTIMET™ - 0.6 Ru	6	−361 ± 2	2.28 ± 0.01	9412 ± 23	23.2 ± 2.0
	3	−320 ± 0	2.75 ± 0.03	6834 ± 31	28.4 ± 1.4
	1	−319 ± 0	4.63 ± 0.23	4749 ± 13	48.4 ± 3.2
STELLITE™ 6B – bulk	6	−192 ± 0	0.03 ± 0.00	97,100 ± 23	0.3 ± 0.0
	3	−283 ± 3	0.01 ± 0.00	98,000 ± 42	0.1 ± 0.0
	1	−189 ± 1	0.02 ± 0.00	93,522 ± 26	0.2 ± 0.0
STELLITE™ 6 - 0 Ru	6	−237 ± 2	0.4 ± 0.22	43,583 ± 68	4.1 ± 0.7
	3	−315 ± 1	0.84 ± 0.03	23,140 ± 71	8.2 ± 1.3
	1	−338 ± 1	8.26 ± 1.00	2637 ± 25	72.3 ± 3.2
STELLITE™ 6–0.3 Ru	6	−425 ± 2	0.88 ± 0.03	24,992 ± 63	8.0 ± 1.3
	3	−336 ± 1	4.94 ± 0.72	4407 ± 76	43.3 ± 2.4
	1	−344 ± 1	5.94 ± 1.00	3660 ± 25	52.4 ± 3.4
STELLITE™ 6–0.6 Ru	6	−249 ± 2	0.41 ± 0.02	53,562 ± 42	4.1 ± 0.1
	3	−280 ± 2	0.64 ± 0.02	30,378 ± 20	6.2 ± 0.2
	1	−359 ± 1	1.10 ± 0.04	1967 ± 16	97.4 ± 2.7
Mild steel	6	−707 ± 2	26.40 ± 2.40	1144 ± 12	262.3 ± 2.0
	3	−726 ± 1	25.00 ± 2.10	941 ± 75	284.3 ± 2.4
	1	−724 ± 1	29.60 ± 3.10	402 ± 123	336.1 ± 2.6

The ULTIMET™ and STELLITE™ 6B bulk alloys also demonstrated similar active-passivation (Fig. 3) to the coatings (Fig. 2) but with pitting regions from log (current density (μA/cm^2)) = 0.5 to 10,000. With decreased pH, current densities shifted to less positive values for ULTIMET™ (Fig. 3 a), although pH 1 and 3 were similar, while there was no discernible trend for STELLITE™ 6B (Fig. 3 b). Conversely, the passivity of STELLITE™ 6B improved when the pH was decreased. After the transpassive region, the curves also overlapped (Fig. 3), indicating similar corrosion resistance of the alloys, even though the microstructures of the alloys were fairly different [2].

Table 2 shows corrosion potentials (E_{corr}), current densities (i_{corr}), linear polarisation resistances (R_p) and corrosion rates of ULTIMET™ and STELLITE™ 6 coatings with 0 Ru, 0.3 and 0.6 Ru in synthetic mine water at 6, 3 and 1 pHs.

The corrosion behaviour of ASTM A516 mild steel at different pH values of synthetic mine water (Fig. 3 c) was similar. At all pH values, mild steel showed active and pseudo-passivation (i.e., unstable or apparent passivation) behaviour from −500 mV to 1200 mV possibly due to pseudo-passive films formed on the surface [15,20,21], which reduced further corrosion by stopping the anodic dissolution reaction at high potentials [22]. This suggests that mild steel suffered general corrosion without true passivation in the synthetic mine water. Figs. 2 and 3 show that the bulk alloys had more positive potentials and lower current densities than the coatings at all pH values.

The results for linear polarisation resistance (R_p) showed that each coating experienced high R_p at high pH values (Table 2). The R_p decreased with decreased pH because of the breakdown of the protective oxide layer, exposing the alloys to the corrosive medium. The ULTIMET™- 0.3 Ru and 0 Ru coatings had the highest R_p, (90,533 Ω cm^2 and 80,967 Ω cm^2), and the lowest corrosion rates (3 μm/y for both), although at different pH, while ULTIMET™ - 0 Ru had the lowest R_p (1643 Ω cm^2) corresponding to its highest corrosion rate (137 μm/y) at pH 1. Fig. 4 shows steeper slopes (i.e., an incline or increase in the corrosion current with respect to the E_{corr}) (e.g., ULTIMET™- 0 Ru and STELLITE™ 6 - 0 Ru at pH 1), indicating high corrosion rates and shallower slopes (e.g., ULTIMET™- 0.3 and STELLITE™ 6–0.6 Ru at pH 6), indicating low corrosion rates. Table 2 shows mild steel had increased current density and decreased R_p when the pH was decreased, giving increased corrosion rates.

Fig. 5 a) shows the effect of the pH and different Ru additions (Fig. 5 b) on the corrosion rates. Generally, the corrosion rates increased when the pH decreased, and for both ULTIMET™ and STELLITE™ 6 (Fig. 5 a), the corrosion rates decreased with increased added Ru (Fig. 5 b). The corriosn rates for coatings were much lower than for the midl steel, as expected (Fig. 5 b). Although it would have been expected that the corrosion rates would decrease with increasing Ru content, for ULTIMET™ – 0.6 wt% Ru at pH 6 it increased. STELLITE™ 6 had a minimum corrosion rate for 0.3 wt% Ru, and ULTIMET™ had a maximum for 0,3 wt% Ru. Considering pH (Fig. 5 b), the highest corrosion rates were for lower pH as expected, except for STELLITE™ 6 with 0.3 wt% Ru which had the highest corrosion rate at pH 3. The highest corrosion rates were for pH 1 for ULTIMET™, and the lowest corrosion rates were for pH 6 for STELLITE™ 6. However, all coatings showed higher corrosion rates when the pH was decreased. The highest corrosion rates was at pH 1, and then pH 3 and 6, as expected.

Fig. 6 shows the microstructures of the ULTIMET™ coating samples before (Fig. 6a–c) [2] and after (Fig. 6d–f) the corrosion tests, while Fig. 7 shows the microstructures of the STELLITE™ 6 samples before (Fig. 7a–c) [2] and after (Fig. 7d–f) the corrosion tests. There were cracks on grain boundaries, which were not observed in the uncorroded samples, but the Ru was not affected.

Tables 3 and Table 4 show EDX analyses of the surfaces of the samples after the corrosion tests at pH 1 (Fig. 8). The elements for which there was no difference in Tables 3 and 4 were either from the test solution or were not measured on the samples before corrosion tests, while a positive difference showed that these elements were little affected by corrosion (i.e., still present on the surface in high amounts). Elements with negative difference were those that had been removed from the surface, i.e., had been corroded.

Ruthenium was not detected after corrosion tests (apart from the STELLITE™ 6–0.6 Ru coating), probably due to the volume detection limit of ~1 wt% [23,24] and also the areas of analyses were small and did not include where Ru occurred because it was not homogeneously distributed [2]. The large amount of Cr and O on the surfaces of both coatings and the presence of Ru on the STELLITE™ 6–0.6 Ru coatings indicated a chromium oxide film formed on the surfaces, which protected them against corrosion [14], as seen from the lower corrosion rates from the polarisation curves in Fig. 2.

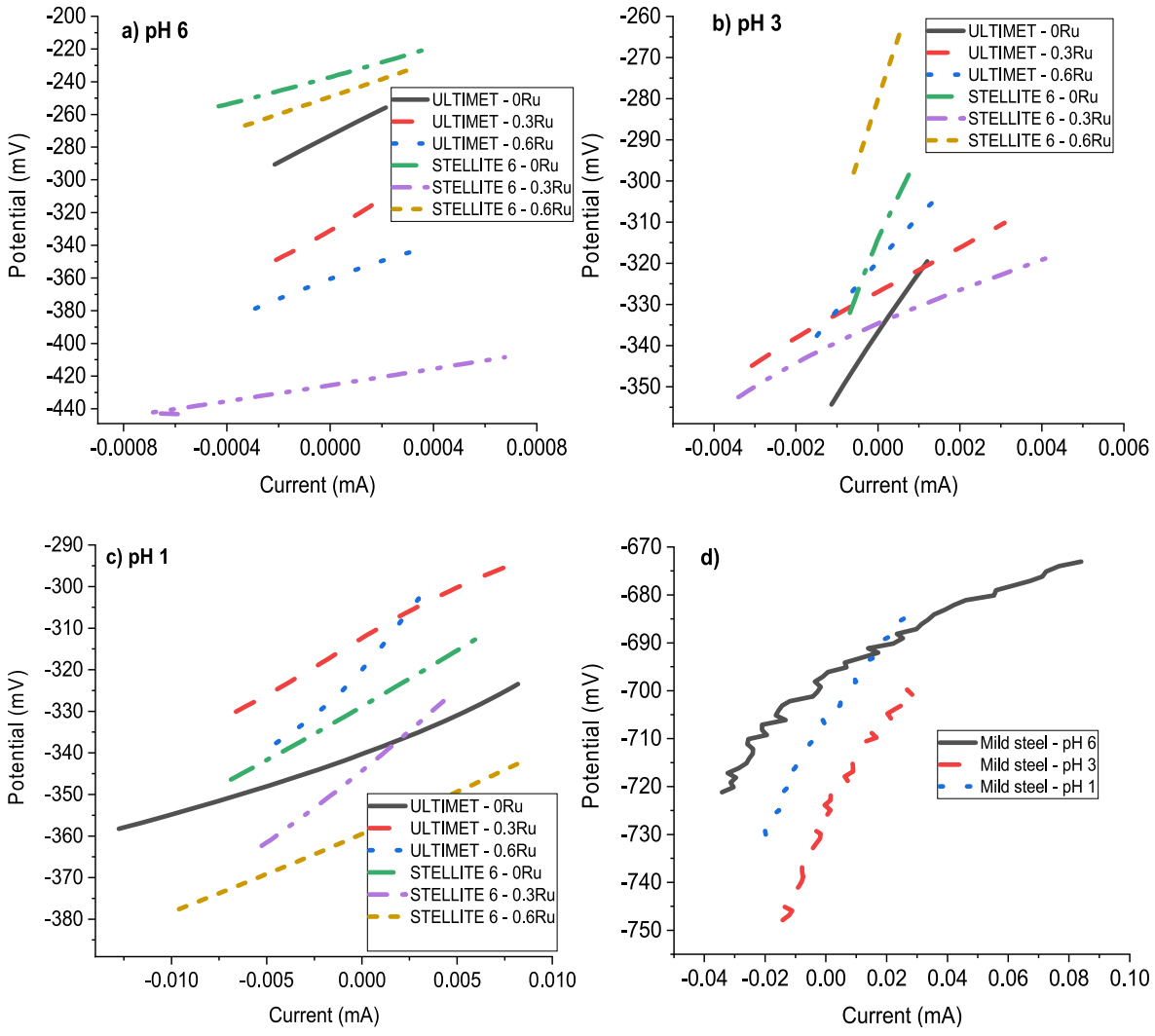

Fig. 4. Linear polarisation resistance plots of ULTIMET™ and STELLITE™ 6 coatings and mild steel in synthetic mine water at: (a) pH 6, (b) pH 3 and pH 1, showing steeper slopes at pH 1 than pH 3 and 6.

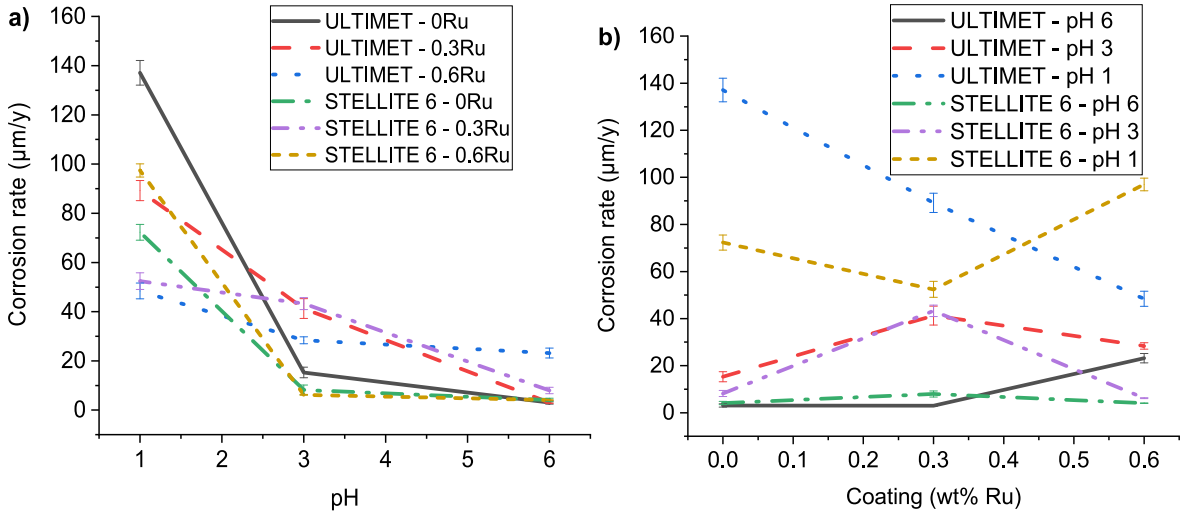

Fig. 5. Effect of: (a) pH and (b) ruthenium content on corrosion rates of ULTIMET™ and STELLITE™ 6 coatings at pH 6, 3 and 1.

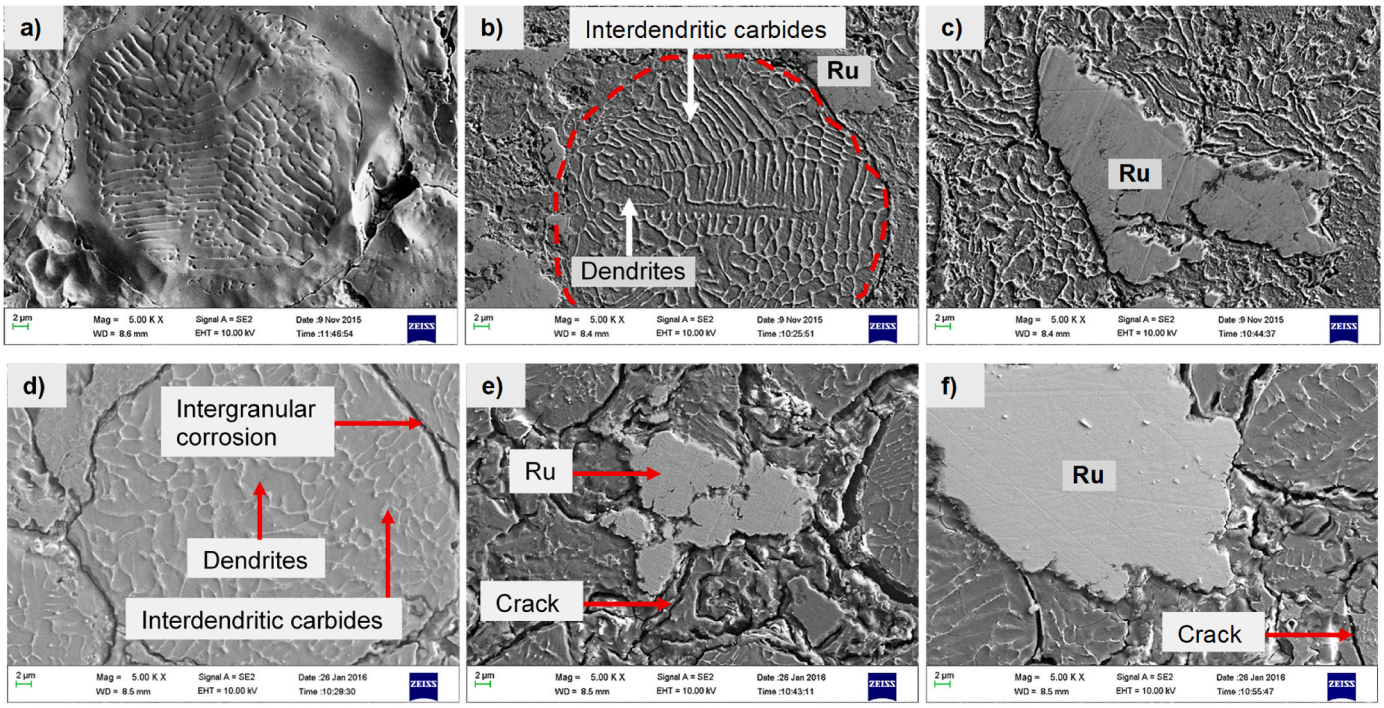

Fig. 6. SEM - SE micrographs of samples before corrosion tests showing the surfaces of ULTIMET™ coatings with: (a) 0 Ru, (b) 0.3 wt% Ru, and (c) 0.6 wt% Ru, with dendrites and interdendritic carbides [2] and after potentiodynamic polarisation in synthetic mine water at pH 1, showing cracks, intergranular corrosion and unaffected ruthenium in ULTIMET™ coatings with; (d) 0 Ru, (e) 0.3 Ru and (f) 0.6 Ru.

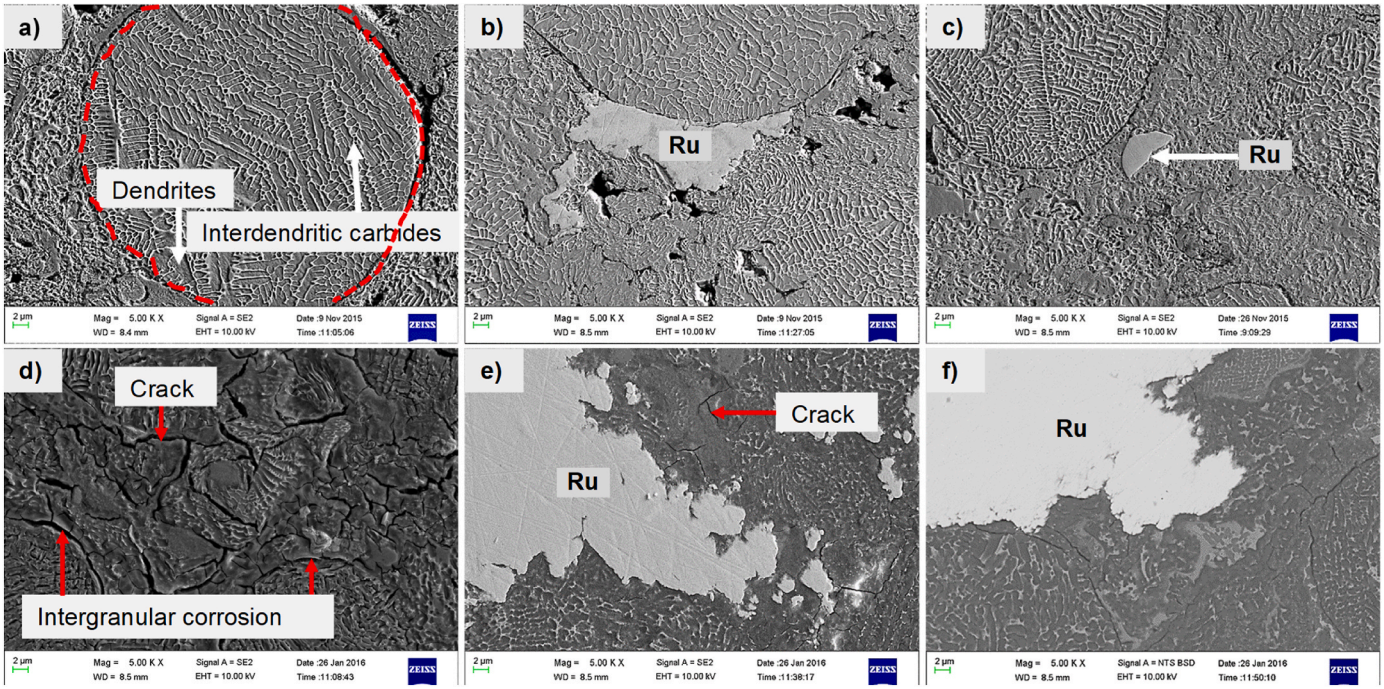

Fig. 7. SEM - SE micrographs of the surfaces of STELLITE™ 6 coatings samples with: (a) 0 Ru, (b) 0.3 wt% Ru, and (c) 0.6 wt% Ru before corrosion tests, showing dendrites and interdendritic carbides [2] and after potentiodynamic polarisation in synthetic mine water at pH 1, showing cracks, intergranular corrosion and unaffected ruthenium in STELLITE™ 6 coatings with; (d) 0 Ru, (e) 0.3 Ru and (f) 0.6 Ru.

4. Discussion

4.1. Corrosion of the alloys and coatings

The OCP results (Fig. 1) showed that the ULTIMET™ coatings were slightly more stable than the STELLITE™ 6 coatings, since they had a stronger passivation tendency, shown by their more stable OCP values [25]. The corrosion rates of both samples at pH 1 were higher than at pHs 3 and 6, due to more chlorides in the solution [10,13,14]. Both ULTIMET™ (Fig. 6) and STELLITE™ 6 (Fig. 7) coatings showed general and intergranular corrosion, with corrosion products and cracks on the surfaces. Figs. 6 and 7 also show that the grain boundaries were more

Table 3
EDX analyses (wt%) of the ULTIMET™ coating surfaces of Fig. 8 after potentiodynamic polarisation in synthetic mine water at pH 1 at ambient temperature, showing the differences between uncorroded [2] and corroded samples.

Element (wt%)	Coating					
	ULTIMET™−0 Ru	% difference	ULTIMET™ −0.3 Ru	% difference	ULTIMET™ −0.6 Ru	% difference
O	13.7 ± 0.4	[a]N/M	17.1 ± 1.0	[a]N/M	17.9 ± 1.0	[a]N/M
Si	0.3 ± 0.0	0	0.3 ± 0.1	50	0.3 ± 0.1	−57.1
S	1.2 ± 0.2	[a]N/M	1.5 ± 0.2	[a]N/M	1.5 ± 0.3	[a]N/M
Cl	0.2 ± 0.1	[a]N/M	[a]N/M	[a]N/M	[a]N/M	[a]N/M
Cr	31.1 ± 1.0	11.1	35.1 ± 1.0	21	35.2 ± 1.3	19.3
Fe	5.4 ± 2.0	2600	0	−100	4.3 ± 2.3	0
Co	33.6 ± 1.0	−32.8	29.0 ± 1.0	−44.2	26.2 ± 1.0	−46.3
Ni	8.2 ± 0.2	−36.9	7.6 ± 0.2	−36.7	6.4 ± 1.0	−47.9
Mo	3.8 ± 0.4	−15.6	4.4 ± 0.4	10	3.8 ± 1.0	−15.6
Ru	0	0	0	−100	0	−100
W	2.6 ± 0.2	30	4.9 ± 0.3	145	4.2 ± 0.4	110

[a] N/M = not measured before corrosion tests.

Table 4
EDX analyses (wt%) of the STELLITE™ 6 coating surfaces of Fig. 8 after potentiodynamic polarisation in synthetic mine water at pH 1, at ambient temperature, showing the differences between uncorroded [2] and corroded samples.

Element (wt%)	Coating					
	STELLITE™ 6–0 Ru	% difference	STELLITE™ 6–0.3 Ru	% difference	STELLITE™ 6–0.6 Ru	% difference
O	18.4 ± 1.0	[a]N/M	16.9 ± 1.0	[a]N/M	11.5 ± 8.0	[a]N/M
Si	0.6 ± 0.0	−14.3	0.5 ± 0.1	−28.6	0.5 ± 0.1	−28.6
S	1.6 ± 0.1	[a]N/M	0.8 ± 0.1	[a]N/M	0.7 ± 0.0	[a]N/M
Cl	1.8 ± 0.2	[a]N/M	0.8 ± 0.2	[a]N/M	0.5 ± 0.1	[a]N/M
Cr	36.7 ± 1.3	10.9	33.8 ± 2.0	2.1	32.8 ± 3.0	7.6
Fe	0	0	22.0 ± 2.0	700	18.0 ± 3.3	−100
Co	18.2 ± 1.2	−65.7	17.6 ± 1.0	20.9	24.5 ± 1.3	−55.6
Ni	14.0 ± 0.4	311.8	2.0 ± 0.3	−41.2	2.3 ± 0.3	−36.1
Mo	0	−100	0	−100	0	−100
Ru	0	0	0	−100	0.3 ± 0.1	−80
W	8.7 ± 0.3	107.1	5.7 ± 0.3	50	5.3 ± 1.0	103.8

[a] N/M = not measured before corrosion tests.

susceptible to corrosion [26]. The dendrites were attacked less than the interdendritic carbides, and Ru was least attacked (Figs. 6 and 7), which shows that the coatings need to be more homogeneous. Smolenska [6] found that under sulphidation and within a cobalt-based clad layer, the carbides decomposed, and there was severe corrosion along the dendrite boundaries, albeit at higher temperatures (800 °C) than this investigation and with sulphur partial pressures (10^{-8} and 10^{-10} atm). The carbides acted as anodes to the rest of the matrix, and they were attacked preferentially [18,19], and they were more in the STELLITE™ 6, hence the low corrosion rates than the ULTIMET™ samples (Table 2, Figs. 6 and 7).

At high pH, protective films formed (Figs. 2 and 3), inhibiting the diffusion of hydrogen ions, resulting in low corrosion rates (Table 2). Conversely, at low pH, these films were disrupted by the evolution of hydrogen ions, exposing the metal to the surrounding solution, increasing oxygen depolarisation, thereby increasing corrosion rates [21]. Increased chloride and sulphate ions in the solution increased the corrosion rate, as these ions break down the passive layers (from 750 mV, Fig. 2), and accelerate corrosion [3,27,28].

The wide range of spontaneous passivation behaviour (−250 mV–750 mV) at pH 3 and pH 1 for coatings (Fig. 2) and bulk alloys (Fig. 3) was associated with the formation of protective thin films of Cr_2O_3 on the surface at low pH [3,10,29]. This behaviour was more stable at pH 6 (~150–900 mV) as high pH enhances passivation, forming a more stable and protective oxide layer on the surface and reducing corrosion [25,30]. Pitting potentials were between 670 mV and 900 mV, although no pits were found by SEM, although they could have been hidden by the surface cracks on the coatings (Figs. 6 and 7).

The corrosion mechanisms of the coatings were similar to those of the bulk alloys. However, the corrosion rates of the bulk alloys were much lower than for the coatings (Table 2), because the bulk alloys were more homogeneous [2]. However, the bulk alloys were susceptible to pitting corrosion (Fig. 3) and were also less hard [2]. The coatings with Ru additions, especially STELLITE™ 6–0.6 Ru, had better hardness and corrosion rates and could be suitable candidates to replace the bulk alloys and to protect mild steel in many industrial applications, including slurry pump components such as casings, sleeves and valves or orthopaedic implants [31,32].

4.2. *Effect of ruthenium on corrosion of the coatings*

The additions of ruthenium to ULTIMET™ and STELLITE™ 6 coatings gave little difference in corrosion rates (Figs. 2 and 4), especially at pH 6 with the worst corrosion rates at pH 1, with corrosion at the edges of the globular particles (Figs. 6 and 7). The small difference was due to similar corrosion behaviour of the two cobalt-based coatings: STELLITE™ 6 (Co–Cr–W–Fe–Ni–Mo) and ULTIMET™ (Co–Cr–Ni–Mo–Fe–W). The Ru contents were probably not accurately analysed, because EDX is only accurate to within ~1 wt% [24], and also because of the inhomogeneous Ru distribution. Additionally, Ru was lost during spray coating of ULTIMET™ (although it was apparently not lost for STELLITE™ 6), although this apparent loss was most likely due to the inhomogeneous distribution of the powders during mixing and spray coating, especially since Ru is heavier than the other elements.

Comparison of the corrosion behaviour of all the alloys (Fig. 5) did not always show the least corrosion with the highest Ru content, because STELLITE™ 6 and ULTIMET™ had higher corrosion rates for 0.6 wt% Ru than for 0.3 wt% Ru (Fig. 5 b), and ULTIMET™ with 0.6 wt% Ru also

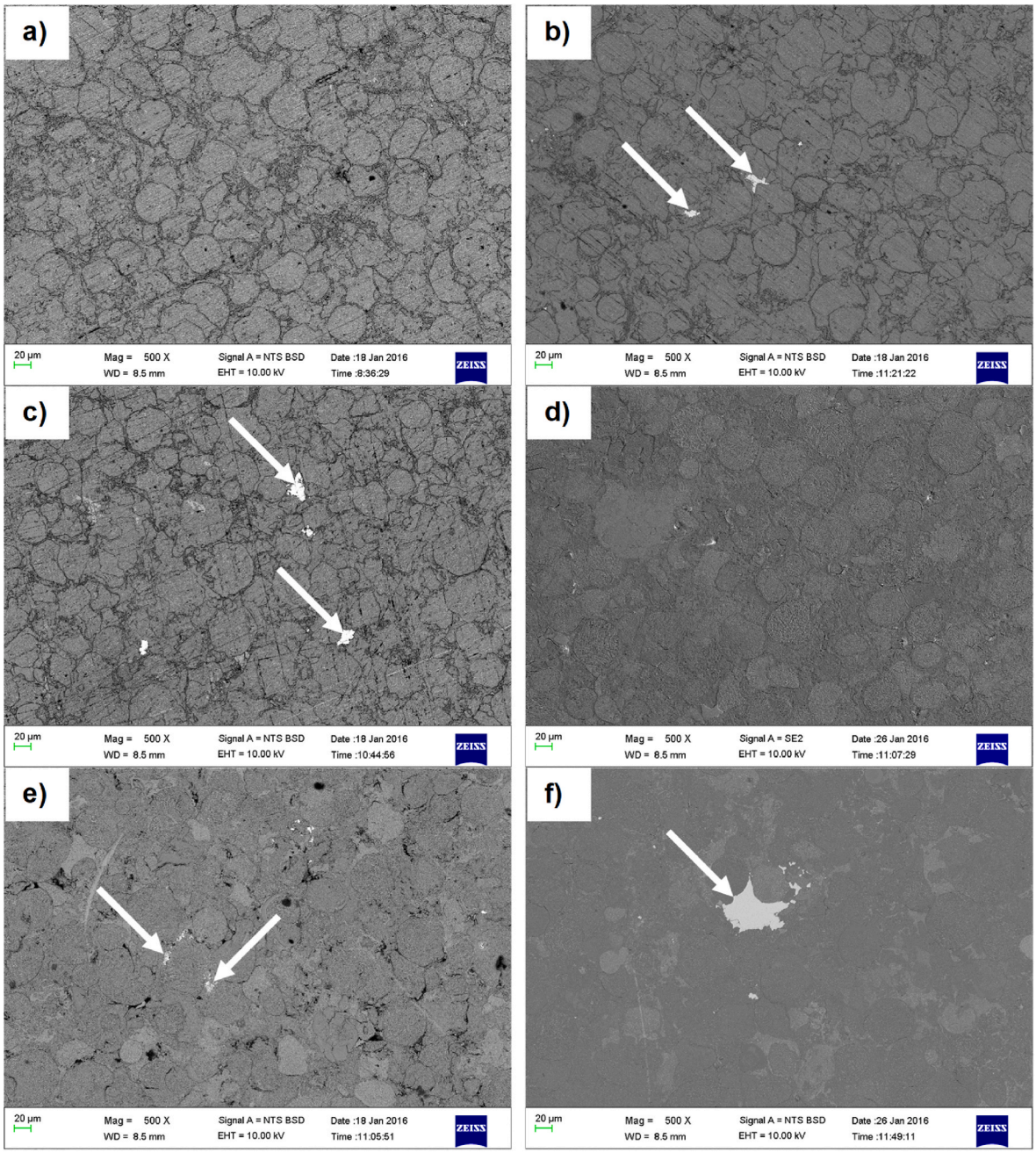

Fig. 8. SEM-BSE images of samples after corrosion tests in synthetic mine water at pH 1, showing the surfaces where EDX analyses were taken (500×) for ULTIMET™ coatings with nominal; (a) 0 Ru, (b) 0.3 Ru, (c) 0.6 Ru, and STELLITE™ 6 coatings: with nominal (d) 0 Ru, (e) 0.3 Ru, f) 0.6 Ru. The arrows show ruthenium.

had a higher corrosion rate at pH 1 than pH 3 and pH 6. This was probably due to the inhomogeneity of Ru, even though adding ruthenium was beneficial for the corrosion resistance of the coatings in the active-passive region transitions and increased passivity ranges (~250 mV–0 mV) [9–14]. These transitions (Figs. 2 and 3) were also due the formation of chromium oxide layers (Fig. 3) on the surface of the coatings. The highest corrosion rates were for pH 1, as expected. The pH 6 would be expected to give the lowest corrosion, as it did for STELLITE™ 6, but there was overlap between pH 3 and 6 for ULTIMET™ which was probably due to both inhomogeneity and loss of Ru (during powder mixing, powder feeding or spray coating), and the inhomogeneity of the carbide distribution [2,33,34], since the coating carbides were not detected by XRD [2]. However, it was expected that small amounts of Ru would dissolve in Co–Cr matrices [35], since at high temperature Ru dissolves in the (Cr) solid solution [35], although the solvus slopes and less dissolves at lower temperatures. However, the Ru did not dissolve in the matrices as shown by the microstructures (Figs. 6 and 7), since Ru was observed as almost pure Ru regions, which suggests that at ambient temperatures, little Ru dissolves in the matrices. This explains the unexpected results when the Ru content did not always give better corrosion resistance.

The increased corrosion rate with increasing Ru content for ULTIMET™ – 0.6 wt% Ru at pH 6 (Table 2) was similar to the effect of Ru additions to stainless steels [14], and to WC–Co cemented carbide alloys [36]. Both studies concluded that increased Ru from 2% to 3% did not yield significant improvements to the corrosion resistance. The reason why increased Ru did not increase the corrosion resistance was that it was not homogeneously distributed in the matrices (Figs. 6 and 7). It must be remembered that Ru is expensive, so it is advantageous to add as little as possible to achieve the improved corrosion resistance [37].

5. Conclusions

The effect of the additions of 0.3 and 0.6 wt% ruthenium on corrosion of ULTIMET™ and STELLITE™ 6 in synthetic and acidified synthetic mine water was studied using potentiodynamic polarisation. Both coatings displayed active-passive transition behaviour. The corrosion resistance of the coatings reduced as the acid concentration increased, as expected. Adding Ru to the coatings reduced the active-passive transition. The lowest corrosion rate was for the STELLITE™ 6 coating with nominal 0.6 wt% Ru at pH 6 and 3. Increased Ru contents in both ULTIMET™ and STELLITE™ 6 coatings increased the hardness. STELLITE™ 6–0.6 Ru was the best coating due to its good corrosion resistance and the highest hardness, and may be used to protect slurry pump components, cutting tools, chemical processing and in marine environments.

CRediT authorship contribution statement

Silas I. Hango: Writing – original draft, Visualization, Validation, Methodology, Investigation, Formal analysis, Data curation, Conceptualization. **Lesley A. Cornish:** Writing – review & editing, Supervision. **Josias W. van der Merwe:** Writing – review & editing, Supervision, Formal analysis. **Lesley H. Chown:** Writing – review & editing, Supervision. **Frank P.L. Kavishe:** Conceptualization, Supervision, Writing – review & editing.

Declaration of competing interest

The authors declare that they have no known competing financial interests or personal relationships that could have appeared to influence the work reported in this paper.

Data availability

Data will be made available on request.

Acknowledgements

The authors wish to acknowledge the financial support received from the African Materials Science and Engineering Network (A Carnegie-IAS RISE network), as well as Weartech Pty (Ltd) and Fe Powder Supplies (Pty) Ltd, Johannesburg, South Africa for the supply of ULTIMET™ and STELLITE™ 6 powders, Thermalspray (Pty) Ltd, Olifantsfontein, South Africa for the use of the HVOF facilities, SGS South Africa (Pty) Ltd, Johannesburg for XRD analyses, Mintek, Randburg, Johannesburg, South Africa for corrosion experiments and Multi Alloys, Midrand, South Africa, for the supply of the ULTIMET™ and STELLITE™ 6B alloys.

References

[1] J.H. Hong, F.Y. Yeoh, Mechanical properties and corrosion resistance of cobalt-chrome alloy fabricated using additive manufacturing, Mater. Today Proc. 29 (2019) 196–201, https://doi.org/10.1016/j.matpr.2020.05.543.
[2] S.I. Hango, L.A. Cornish, L.H. Chown, J.W. van der Merwe, F.P.L. Kavishe, Sliding wear resistance of the cobalt-based coatings, ULTIMETTM and STELLITETM 6 with ruthenium additions, Eng. Fail. Anal. 155 (2024) 107717, https://doi.org/10.1016/j.engfailanal.2023.107717.
[3] R. Metikoš-Huković, M. Babić, Passivation and corrosion behaviours of cobalt and cobalt – chromium – molybdenum alloy, Wear 49 (2007) 3570–3579, https://doi.org/10.1016/j.corsci.2007.03.023.
[4] M. Sebastiani, V. Mangione, D. De Felicis, E. Bemporad, F. Carassiti, Wear mechanisms and in-service surface modifications of a stellite 6B Co – Cr alloy, Wear 290–291 (2012) 10–17, https://doi.org/10.1016/j.wear.2012.05.027.
[5] Hynes International, Ultimet alloy: improved cobalt chromium molybdenum cobalt-base alloy, Alloy Dig. 42 (3) (1993), https://doi.org/10.31399/asm.ad.co0089.
[6] H. Smolenska, Cobalt base clad layer resistance on the corrosion under low sulfur pressure, Solid State Phenom. 165 (2010) 173–176. https://doi.org/10.4028/www.scientific.net/SSP.165.173.
[7] J. Chen, H. Dong, Corrosion and corrosion wear behaviour of plasma carburised stellite 21 Co – Cr alloy, Tribol. Mater. Surface Interfac. 3 (2009) 24–30, https://doi.org/10.1179/175158309X419043.
[8] D. Sri Maha Vishnu, J. Sure, Y. Liu, R. Vasant Kumar, C. Schwandt, Electrochemical synthesis of porous Ti-Nb alloys for biomedical applications, Mater. Sci. Eng. C 96 (2019) 466–478, https://doi.org/10.1016/j.msec.2018.11.025.
[9] J.H. Potgieter, Alloys cathodically modified with noble metals, J. Appl. Electrochem. 21 (1991) 471–482, https://doi.org/10.1007/BF01018598.
[10] E.S.M. Sherif, J.H. Potgieter, J.D. Comins, L.A. Cornish, P.A. Olubambi, C. N. Machio, Effects of minor additions of ruthenium on the passivation of duplex stainless-steel corrosion in concentrated hydrochloric acid solutions, J. Appl. Electrochem. 39 (2009) 1385–1392, https://doi.org/10.1007/s10800-009-9814-5.
[11] S.C.K. Banda, J. van der Merwe, Effect of small additions of ruthenium on pitting corrosion resistance of LDX2101 duplex stainless steel, Corrosion Eng. Sci. Technol. 49 (2014) 32, https://doi.org/10.1179/1743278213Y.0000000101.
[12] J.H. Potgieter, J. Thomson, F.V. Adams, A.S. Afolabi, Effect of additions of Ru and Pd on the electrochemical behaviour of austenitic stainless steel in organic acids, Int. J. Electrochem. Sci. 9 (2014) 6451–6463, https://doi.org/10.1016/S1452-3981(23)10901-1.
[13] O.A. Olaseinde, J.W. van der Merwe, L.A. Cornish, L.H. Chown, P.A. Olubambi, Electrochemical studies of Fe-21Cr-1Ni duplex stainless steels with 0.15 Wt% ruthenium at different temperatures, J. South. African Inst. Min. Metall. 7A (2012) 535–538. http://www.scielo.org.za/pdf/jsaimm/v112nspe/07.pdf.
[14] P.A. Olubambi, J.H. Potgieter, L.A. Cornish, Corrosion behaviour of superferritic stainless steels cathodically modified with minor additions of ruthenium in sulphuric and hydrochloric acids, Mater. Des. 30 (2009) 1451–1457, https://doi.org/10.1016/j.matdes.2008.08.019.
[15] J.W. van der Merwe, F. Moyo, E.M. Phetla, Corrosion behaviour of ruthenium laser surface alloyed austenitic stainless steel in sulphuric acid and sodium chloride solutions, Mater. Corros. 68 (2017) 815–823, https://doi.org/10.1002/maco.201609343.
[16] L. Chipise, P.K. Jain, L.A. Cornish, Influence of Ru on the hardness and fracture toughness of WC-VC-Co alloys, Int. J. Refract. Met. Hard Mater. 77 (2018) 54, https://doi.org/10.1016/j.ijrmhm.2018.07.008.
[17] C. Allen, Corrosion of galvanised steel in synthetic mine waters, Br. Corrosion J. 26 (1991) 93–101, https://doi.org/10.1179/000705991798269288.
[18] V. Marimuthu, K. Kannoorpatti, Corrosion behaviour of high chromium white iron hardfacing alloys in acidic and neutral solutions, J. Bio-Tribo-Corros. 2 (2016) 1–12, https://doi.org/10.1007/s40735-016-0059-7.
[19] R.W. Manuel, Effect of carbide structure on the corrosion resistance of steel, Corrosion 3 (1947) 415–431, https://doi.org/10.5006/0010-9312-3.9.415.
[20] R.A. Rodríguez-Díaz, A.L. Ramirez-Ledesma, M.A. Aguilar-Mendez, J. Uruchurtu Chavarin, M.A. Hernández Gallegos, J.A. Juarez-Islas, Electrochemical corrosion behavior of a Co20Cr alloy in artificial Saliva, Int. J. Electrochem. Sci. 10 (2015) 7212–7226, https://doi.org/10.1016/S1452-3981(23)17343-3.
[21] P.V. Scheers, The effects of flow velocity and pH on the corrosion rate of mild steel in a synthetic minewater, J. South African Inst. Min. Metall. 92 (1992) 275–281. http://saimm.org.za/Journal/v092n10p275.pdf.
[22] W. Li, B. Brown, D. Young, S. Nešić, Investigation of pseudo-passivation of mild steel in CO_2 corrosion, Corrosion 70 (2014) 294–302, https://doi.org/10.5006/0950.
[23] J.I. Goldstein, D.E. Newbury, J.R. Michael, N.W.M. Ritchie, J.H.J. Scott, D.C. Joy, Scanning Electron Microscopy and X-Ray Microanalysis, fourth ed., Springer Nature, New York, USA, 2017 https://doi.org/10.1007/978-1-4939-6676-9.
[24] S. Nasrazadani, S. Hassani, Chapter 2: modern analytical techniques in failure analysis of aerospace, chemical, and oil and gas industries, in: Handbook of Materials Failure Analysis with Case Studies from the Oil and Gas Industry, Butterworth-Heinemann, Elsevier Ltd., 2016, pp. 39–54, https://doi.org/10.1016/B978-0-08-100117-2.00010-8.
[25] A. Mace, P. Khullar, C. Bouknight, J.L. Gilbert, Corrosion properties of low carbon CoCrMo and additively manufactured CoCr alloys for dental applications, Dent. Mater. 38 (2022) 1184–1193, https://doi.org/10.1016/j.dental.2022.06.021.
[26] X. Zhang, Y. Li, N. Tang, E. Onodera, A. Chiba, Corrosion behaviour of CoCrMo alloys in 2 wt% sulphuric acid solution, Electrochim. Acta 125 (2014) 543–555, https://doi.org/10.1016/j.electacta.2014.01.143.
[27] Y. Cui, Y. Qin, D. Dilimulati, Y. Wang, The effect of chlorine ion on metal corrosion behavior under the scratch defect of coating, Int. J. Corros. 2019 (2019) 1–12, https://doi.org/10.1155/2019/7982893Research.
[28] F.M. Ai-Kharafi, W.A. Badawy, J.R. Al-Ajmi, Effect of chloride ions on the corrosion and passivation behaviours of cobalt in neutral solutions, Indian J. Chem. Technol. 6 (1999) 194–201. http://nopr.niscpr.res.in/handle/123456789/16925.
[29] L. Reclaru, H. Lüthy, P.Y. Eschler, A. Blatter, C. Susz, Corrosion behaviour of cobalt-chromium dental alloys doped with precious metals, Biomaterials 26 (2005) 4358–4365, https://doi.org/10.1016/j.biomaterials.2004.11.018.
[30] C.R.C. Lima, M.J.X. Belém, H.D.C. Fals, C.A.D. Rovere, Wear and corrosion performance of Stellite 6® coatings applied by HVOF spraying and GTAW Hotwire cladding, J. Mater. Process. Technol. 284 (2020) 116734, https://doi.org/10.1016/j.jmatprotec.2020.116734.
[31] Z. Que, M. Ahonen, I. Virkkunen, P. Nevasmaa, P. Rautala, Study of cracking and microstructure in Co-free valve seat hardfacing, Nucl. Mater. Energy 31 (2022) 101202, https://doi.org/10.1016/j.nme.2022.101202.
[32] D. Prabhakaran, N. Jegadeeswaran, B. Somasundaram, B.S. Raju, Corrosion resistance by HVOF coating on gas turbine materials of cobalt based superalloy, Mater. Today: Proc. 20 (2020) 173–176, https://doi.org/10.1016/j.matpr.2019.10.102.

[33] S.I. Hango, J.W. van der Merwe, L.H. Chown, F.P.L. Kavishe, L.A. Cornish, Development of wear and corrosion resistant coatings for potential use on sleeves of pumps in a copper mine, in: 6th Regional Conference of Society of Mining Professors, Southern African Institute of Mining and Metallurgy), Johannesburg, South Africa, 2018, pp. 1–16.
[34] S.I. Hango, Failure of Pump Systems Operating in Highly Corrosive Mine Water at Otjihase Mine, PhD Thesis, University of the Witwatersrand, Johannesburg, South Africa, 2018, http://wiredspace.wits.ac.za/handle/10539/25666.
[35] T.B. Massalski, Binary Alloy Phase Diagrams, vol. 1, American Society for Metals, Ohio, USA, 1989, 9780871706218.
[36] J.H. Potgieter, N. Thanjekwayo, P. Olubambi, N. Maledi, S.S. Potgieter-Vermaak, Influence of Ru additions on the corrosion behaviour of WC-Co cemented carbide alloys in sulphuric acid, Int. J. Refract. Met. Hard Mater. 29 (2011) 478–487, https://doi.org/10.1016/j.ijrmhm.2011.02.007.
[37] J.H. Potgieter, W. Skinner, A.M. Heyns, The nature of the passive film on cathodically modified stainless steels, J. Appl. Electrochem. 23 (1993) 11–18, https://doi.org/10.1007/BF00241569.